The relevance of thermal effects during CO2 adsorption and regeneration in a geopolymer-zeolite composite: Experimental and modelling insights

The relevance of thermal effects during CO_2 adsorption and regeneration in a geopolymer-zeolite composite: experimental and modelling insights

M. Boscherini[a,b], F. Miccio[b,*], E. Papa[a], V. Medri[a], E. Landi[a], F. Doghieri[b], M. Minelli[b]

a) Institute of Science and Technology for Ceramics (ISTEC), National Research Council of Italy (CNR), via Granarolo, 64, 48018 Faenza, RA, Italy

b) Department of Civil, Chemical, Environmental and Materials Engineering (DICAM), Alma Mater Studiorum, University of Bologna, via Terracini 28, 40131 Bologna, Italy

* corresponding author: francesco.miccio@cnr.it

Abstract

Low temperature adsorption of carbon dioxide in solid materials is a cost-effective option for implementing decarbonization in a retrofitting plant strategy. Among several natural and artificial sorbents, geopolymer-zeolite composites represent a valid alternative owing to the affinity and synergy between zeolite and the geopolymer binder. Thermal effects are usually associated to CO_2 adsorption in solids: in particular zeolites exhibit values in the range 33 to 40 kJ/mol. The occurrence of the thermal effects (i.e. positive/negative variation of the bed temperature) impacts on the adsorption/desorption behavior and system performance. In this study, the relationship between adsorption/desorption and adsorption bed temperature has been studied in dynamic tests, complemented by thermogravimetric analysis and static sorption experiments. In dynamic tests, the maximum adsorption capacity was 1.40 mmol/g at 20% mol. of CO_2 inlet concentration, whilst it resulted 0.80 mmol/g in a shorter breakthrough test. Correspondingly, the temperature peak during adsorption revealed an increase up to 20 °C. The thermal effect was exploited during desorption with a combined pressure-swing and temperature-swing strategy, leading to a shorter time for sorbent regeneration. A novel numerical model of the adsorption process well fitted the experimental results at different inlet CO_2 concentration, providing insights for process design and optimization.

Keywords

Gas adsorption; CO_2 capture; thermal effect; geopolymer/zeolite composite; transport phenomena model.

1. Introduction

The mitigation of the greenhouse agents in the atmosphere can be firstly addressed by reducing the emissions of anthropogenic carbon dioxide in the environment from power plants or industrial sites such as cement plants. In this context, CO_2 adsorption using solid materials is a suitable and cost effective option for implementing carbon capture at plant site with a retrofitting strategy [1]. The requisites for adsorbent materials are high adsorption capacity for CO_2 and large selectivity towards other gases, along with thermal stability and mechanical resistance in handling and loading operations [2]. Adsorption can be operated either in fixed or in fluidized beds under transient and alternated working conditions. The CO_2 containing gaseous stream is fed to a bed of sorbent until almost complete exhaustion of its adsorption capacity or achievement of breakthrough point after which the CO_2 capture sharply decays [3]. Then, the feed is switched to a second bed, whilst the first one is regenerated by either increasing the temperature or decreasing the pressure. The former strategy is named temperature switch adsorption (TSA), the latter one pressure switch adsorption (PSA). In such a way, the gas separation process occurs in a semi-continuous operation mode. In turn, the breakthrough time is defined as the time when the concentration of the key component reaches a preset threshold value (e.g. 10% of the inlet value), which can be optimized according to sorbent characteristics and operating conditions. In fact, the bed utilization at breakthrough depends on the initial gas concentration, the frontal gas velocity, the bed height-to-diameter ratio [4], as well as on the kinetic rate of the adsorption. In alternative to fixed beds, fluidized beds may accomplish continuous operation through the circulation of the granular sorbent from the adsorption to the regeneration bed [5].

Several materials have been proposed for CO_2 adsorption having CO_2 capacity at nearly standard conditions of temperature and pressure in the range 0.5 – 5.0 mmol/g [1]: activated carbons [6], zeolites [7, 8], organic polymers [9], MOFs [10], geopolymers and their composites [11, 12].

Thermal effects are usually associated to the adsorption of CO_2 in solids as consequence of the establishment of weak forces between the support and the adsorbate. For CO_2 adsorption in zeolite 13X, values in the range 39 to 41 kJ/mol have been measured directly by DSC calorimetry, showing a weak increasing dependence on the adsorption temperature [13]. The isosteric heat of adsorption, representative of the adsorption enthalpy $\tilde{H}_{ads}$ at assigned adsorbate loading *q*, can be calculated from the CO_2 isotherms at different temperatures by the Clausius–Clapeyron equation [14]:

$$\tilde{H}_{ads} = -R\left(\frac{\partial \ln p}{\partial(1/T)}\right)_q \qquad (1)$$

Lee et al. [15] reported $\tilde{H}_{ads}$ values equal to 40.0 kJ/mol at CO_2 loading of 1 mol/kg for a zeolite Na13X, while lower values have been obtained for zeolite Na 4A, ranging around 33 – 35 kJ/mol [16, 17]

Geopolymers, a class of inorganic materials recently applied as highly porous materials [18], have been used in combination to zeolite phases to produce composite materials for various applications: ventilation-filtration, adsorption, pervaporation, water remediation, etc. [19]. In particular, a CO_2 sorbent produced by the inclusion of zeolite Na13X in a geopolymer matrix has been investigated by thermogravimetric analysis and direct adsorption tests by the pressure decay technique [12]. The results indicated interesting capacity and selectivity values for carbon dioxide capture in the low to medium range of concentration (up to 20% mol.), thanks to a synergistic effect between the geopolymer matrix and the zeolite on CO_2 adsorption, which allowed for an enhanced CO_2 capacity with respect to a simple additive law based on the capacity of neat geopolymer and zeolite. Furthermore, the geopolymeric matrix strongly improves the mechanical resistance of the composite sorbent in comparison to zeolite alone, with no significant impact on gas diffusion, making it possible to produce granules suitable for fluidized bed operation [20].

Therefore, the study in differential adsorption bed fed with continuous flow of a gas mixture (e.g. CO_2/N_2) represents a further step towards real operation conditions of the studied material. Tests in differential adsorption beds allow the determination of the breakthrough time that is of paramount relevance for the design of the separation unit in the industrial plant [21]. Furthermore, the measurement of the temperature inside the sorbent bed provides insights into the thermal effects during mass transfer and suggests possible strategies to enhance the process performance [22-24]. In this respect, this research is a progress of the activity already done by the authors [12], providing novel CO_2 static adsorption results at different temperatures in the most promising zeolite-geopolymer sorbent previously studied [12]. Transient results obtained by thermo-gravimetric technique and CO_2 adsorption in a differential bed allowed to study the dynamic response of the sorbent during adsorption/desorption. Particular focus is on the thermal effect associated to the mass transfer phenomena, which is object of mathematical simulation by an originally developed numerical model.

2. Methods

2.1 Materials preparation

The geopolymer-zeolite composite ($NaG_{1.2}Z$) and the reference sodium-based geopolymer matrix ($NaG_{1.2}$) have been fabricated using the same formulations and following the same procedure reported on previous works [12, 25]. Briefly, $NaG_{1.2}$ with theoretical Si:Al molar ratio equal to 1.2 has been prepared by mechanically mixing metakaolin M1200S (Imerys) with a sodium hydroxide solution (10 M). The composite $NaG_{1.2}Z$ has been obtained adding 27 wt. % of Na13X zeolite powder, $Na_{86}[(AlO_2)_{86}(SiO_2)_{106}]\cdot H_2O$ (Sigma-Aldrich, average particle size = 2 μm, specific surface area = 791 m^2/g and pore volume = 301 mm^3/g) to the $NaG_{1.2}$ slurry. Both slurries have been cured for 24 h at 80 °C in closed vessels and for other 24 h at 80 °C in open vessels. After consolidation,

the $NaG_{1.2}Z$ and $NaG_{1.2}$ monoliths obtained have been crashed into granules and sieved in the ranges 400-630 µm.

The main properties of $NaG_{1.2}Z$ and $NaG_{1.2}$ are summarized in Table 1, while Fig. 1 shows the microstructure of the materials produced, as well as that of Na13X zeolite powder. Previous works [12, 25] demonstrated the formation of a substantially high amount of zeolite NaA with cubic phase in $NaG_{1.2}$ and $NaG_{1.2}Z$, namely 65 and 40 mol. %, respectively. In $NaG_{1.2}Z$ (Fig. 1 b and c), the NaA cubic phase is intimately mixed with the multifaceted/rhomboidal Na13X zeolite phase. Indeed, as shown in Fig. 1d, Na13X presents crystals with no distinct edges compared to NaA cubic phase.

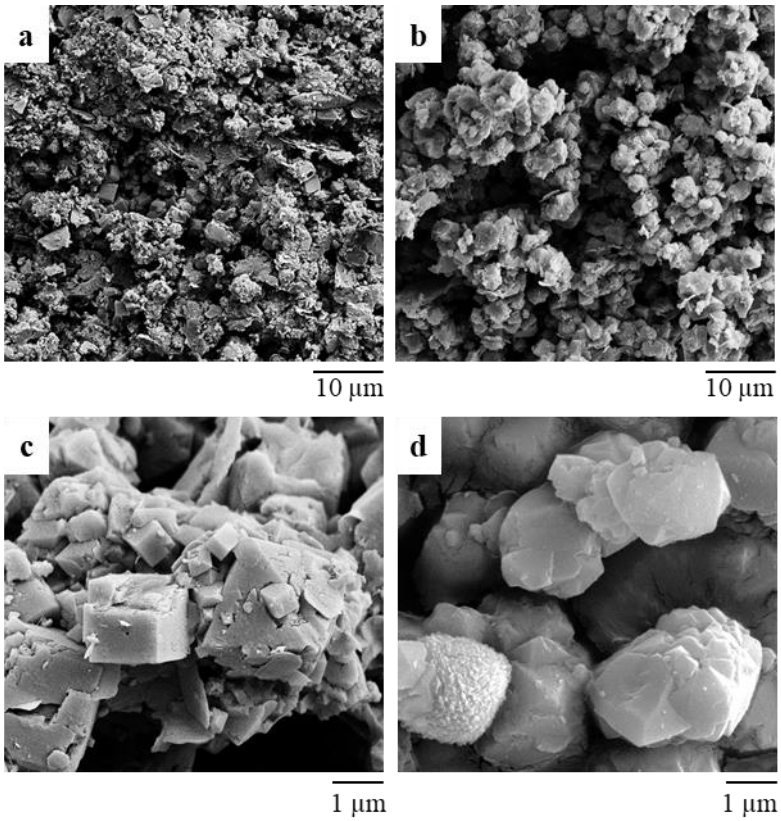

Figure 1. SEM micrographs of geopolymer matrix $NaG_{1.2}$ (a), geopolymer-zeolite composite $NaG_{1.2}Z$ at different magnifications (b, c) and Na13X zeolite powder used as filler (d).

Table 1. Bulk density, porosity by mercury intrusion porosimetry MIP (*), specific surface area (SSA) by N_2 adsorption/desorption at 77 K (§) and compressive strength σ of the materials [12, 25].

Sample	**Zeolite Na13X content** (wt. %)	**Bulk density** ($g\ cm^{-3}$)	**Porosity** * (%)	**SSA**§ ($m^2\ g^{-1}$)	**σ** (MPa)
$NaG_{1.2}$	0.0	1.15	38	13	7.5 ± 0.1
$NaG_{1.2}Z$	27	0.99	47	211	3.0 ± 0.4
Na13X	100	-	-	791	-

2.2 Experimental setup

Static adsorption

Static adsorption experiments have been carried out by means of a volumetric method, in a dedicated pressure decay apparatus already reported in a previous work [26]. Briefly, the adsorbed amount of CO_2 at different pressures is evaluated from the pressure decrease in a calibrated volume (in isothermal conditions) where the adsorbent material is located. Differential sorption steps allow to obtain the adsorption isotherm of the material under investigation at the desired temperature. A sample of geopolymer-zeolite composite granules (about 1 g), conditioned at 200°C in a vacuum oven, is located in the holder chamber, and further conditioned at 80 °C under vacuum overnight. Afterwards, the sample chamber is filled with a certain amount of pure CO_2, at T = 35, 45, 55, 65 and 75 °C. The consequent adsorption in the solids causes a pressure decrease over time. The adsorption capacity is obtained when the final pressure in the chamber achieves an asymptotic value, by using ideal gas law equation for the determination of the adsorbed mole number. The procedure is repeated by increasing stepwise the gas pressure up to approximately 1 bar.

Thermogravimetry

The adsorption/desorption of CO_2 has been also investigated through a thermogravimetric method using a Netzsch STA449 Jupiter operating at 35°C under flowing 20/80% mol. CO_2/N_2 gas

mixture, using the same protocols used in previous researches [12, 25]. The samples (80-100 mg) were tested after performing an instrument calibration test in the same analysis conditions. The analysis program included a conditioning treatment under flowing N_2 (0.04 NL/min) at 100°C for 60 min and cooling to 35°C followed by an isothermal step of 20 min to obtain stable conditions. Then the first adsorption step was recorded adding CO_2 stream (0.01 NL/min) for 20 min to the N_2 flux. Adsorption/desorption cycles were repeated 8 times to assess the reproducibility. The adsorbed CO_2 percent (wt.%) was calculated as the ratio between the adsorption weight gain and the weight of the material after the previous desorption step (baseline weight). The use of a TG/DSC sample carrier allowed to simultaneously detect gravimetric and thermal (enthalpy) phenomena.

Differently to equilibrium adsorption described above, these tests are carried out in a dynamic configuration, by swinging feed CO_2 partial pressure, making use of a limited amount of sorbent Therefore, the results will provide preliminary indications about the sorbent working capacity, coupled with data on the thermal effects associated.

Dynamic adsorption

Figure 2 illustrates the layout of the experimental apparatus used for the dynamic adsorption tests. The feed gas mixture is obtained from bottles of pure N_2 and CO_2 by means of two electronic mass-flow controllers (Brooks Instruments mod. 5850S) and a quick switching valve on the CO_2 line allows to start the breakthrough experiment. The lowest CO_2 feed concentration (5%), out of reach for the electronic controller, has been obtained using a manual mass-flow meter (Key Instruments, 0.5 – 1.0 NL/min). The fixed bed is made of a glass tube (25.7 mm ID, H=200 mm) with an external electric coil (iron wire 0.2 mm tick) applied at 24 V DC by an electronic PID controller (Eurotherm 0316) for thermal heating. A Teflon tape was applied with multiple layers at

the external surface for electric and thermal insulation. A K-type thermocouple is inserted in the adsorbing bed from the exit end for temperature measurement. The determination of the gas concentration, i.e CO_2, leaving the adsorbent bed is carried out by a continuous multicomponent gas analyzer (Testo 350, Testo SE & Co. KGaA, Italy). A personal computer is used for data, i.e. CO_2 outlet concentration and adsorption bed temperature, monitoring and acquisition.

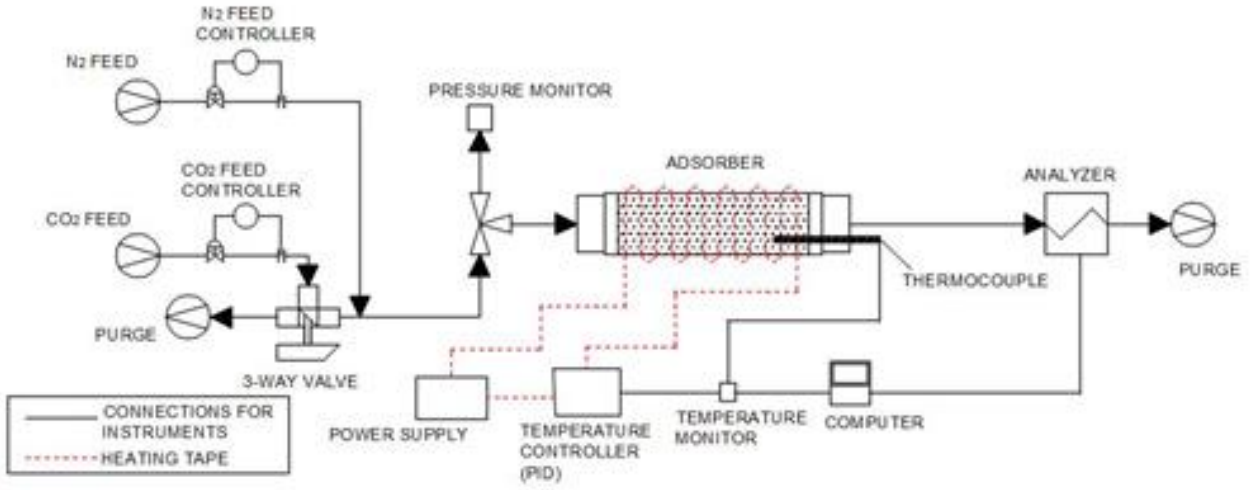

Figure 2. Layout of the test rig for dynamic adsorption/desorption tests.

Before each series of tests, the solid sorbent is regenerated by a thermal treatment, within the packed bed at T = 130 ± 5 °C for at least 90 min, under continuous N_2 flux (0.5 ± 0.05 NL/min). The selected regeneration process has been found to be effective in the removal of both residual CO_2 and water. Before each test, the feed concentration is also checked in the analyzer, by-passing the sorbent bed, to verify the calibration of the system and to ensure the correct functioning of the flowmeters. The switch between adsorption and desorption steps is obtained by interrupting the CO_2 feed to the adsorption bed; therefore, while the inert (N_2) flow remains constant, the total mass-flow through the column changed between adsorption and desorption. Consequently, a slight change in pressure (about 1.5 kPa) is detected.

Two different types of dynamic test have been conducted: 1) complete adsorption tests, in which both adsorption and desorption steps are carried out up to completion, with no heating the sorbent bed, and 2) cyclic tests, in which the adsorption steps are carried out up to the breakthrough point (CO_2 outlet concentration equal to 5% that in the feed) and followed by 60 min desorption step (at the desired temperature).

Such sets of measurements complement well equilibrium adsorption and TGA, being very application oriented. Indeed, tests are carried out on a representative amount of sorbent, packed into the adsorption bed, and operative conditions are similar to those employed in real application.

The total adsorbed and desorbed quantities of carbon dioxide are calculated through the numerical integration of the CO_2 concentration profile, assuming ideal gas behaviour for the gas phase. Mass (molar) balances for the gas phase are derived for N_2 (Eq. 2) and CO_2 (Eq. 3), in the hypothesis that only CO_2 can be adsorbed by the solid sorbent:

$$\dot{n}_{in}\, y_{\mathrm{N_2}}^{\mathrm{in}} = \dot{n}_{out}\, y_{\mathrm{N_2}}^{\mathrm{out}} \tag{2}$$

$$\frac{dn_{CO_2}}{dt} = \dot{n}_{in}\, y_{\mathrm{CO_2}}^{\mathrm{in}} - \dot{n}_{out}\, y_{\mathrm{CO_2}}^{\mathrm{out}} \tag{3}$$

where $\dot{n}$ is the molar flowrate as measured by the mass flow controller (in NL/min), *in* and *out* superscripts denote inlet and outlet conditions, y_i is the molar fraction of component *i*, and n_{CO_2} are the adsorbed CO_2 moles.

Combining Eqs. 2 and 3 and integrating over the time, the total adsorbed moles of carbon dioxide (Eq. 4) and the adsorption capacity q_{CO2} (Eq. 5) can be readily determined:

$$n_{CO_2(t)} = \dot{n}_{in} \int_{t_0}^{t_0+t} \left(y_{\mathrm{CO_2}}^{\mathrm{in}} - y_{\mathrm{CO_2}}^{\mathrm{out}} \frac{1-y_{\mathrm{CO_2}}^{\mathrm{in}}}{1-y_{\mathrm{CO_2}}^{\mathrm{out}}} \right) dt' \tag{4}$$

$$q_{CO_2} = \frac{n_{CO_2(t_{ads})}}{m_s} \quad (5)$$

where m_s is the mass of the loaded sorbent and t_a, t_{ads} indicate initial time and duration of the adsorption step, respectively. Eq. 4 has been integrated numerically by using an explicit trapezoidal method, using a constant time step of 1 second. The same integration method has been applied for the calculation of the degree of adsorption (Eq. 6) and desorption (Eq. 7), in which t_{des} represents the duration of the desorption step:

$$\chi_{ads(t)} = \frac{\dot{n}_{in}}{q_{CO_2}^{\max} m_s} \int_{t_0}^{t_0+t} \frac{y_{CO_2}^{\text{in}} - y_{CO_2}^{\text{out}}}{1 - y_{CO_2}^{\text{out}}} dt' \quad (6)$$

$$\chi_{des(t)} = \frac{\dot{n}_{in}}{q_{CO_2}^{\max} m_s} \int_{t_0+t_{ads}}^{t_0+t_{ads}+t} \frac{y_{CO_2}^{\text{out}}}{1 - y_{CO_2}^{\text{out}}} dt' \quad (7)$$

being $q_{CO_2}^{\max}$ the maximum CO_2 capacity of the solid adsorbent. In turn, the derivatives of the conversion degree ($d\chi/dt$) have been approximated by the difference quotient of the conversion degree calculated over each time step.

2.3 Mathematical model

A 1-D numerical model for prediction of the time behaviours of conversion degree and temperature in the sorbent bed has been developed and implemented in FORTRAN. The model is based on the equations of continuum thermomechanics, and computes the temperature and CO_2 concentration over time along the axial direction of the adsorption bed. The model employs the Peng-Robinson equation [27] to represent the gas phase properties at the desired temperature and pressure, while the adsorption of the active component on the sorbent is described by the

Sips equation [28, 29], a generalized Langmuir model [30] defined on a fugacity basis f_{CO_2}, for the sake of generality:

$$q^*_{CO_2}\left(T, f_{CO_2}\right) = q_\infty\left(T\right)\frac{\left(K_S(T)\, f_{CO_2}\right)^{s(T)}}{1+\left(K_S(T)\, f_{CO_2}\right)^{s(T)}} \tag{8}$$

$$K(T) = \Omega \exp\left(-\frac{\Theta}{RT}\right) \tag{9}$$

$$q_\infty(T) = \alpha \exp\left(-\frac{\theta}{RT}\right) \tag{10}$$

$$s(T) = s_R + s_1 \operatorname{atan}\left(s_2(T - T_\infty)\right) \tag{11}$$

where the seven parameters Ω, Θ, α, θ, s_R, s_1, s_2 are obtained by the interpolation of experimental adsorption isotherms data at different temperature with a linear least squares method.

In the case of interest, near or above room temperature and sub-atmospheric pressure, fugacity coefficient is very near 1, so gas fugacity can be readily replaced by partial pressure. The model, however, defined on fugacity basis, can be employed to describe any kind of adsorption processes, including those at higher pressure, also relevant for chemical engineering and environmental applications.

The model is based on the following simplifying conditions:

- two phases only are considered: the gas phase consisting of CO_2 and N_2, and the solid phase, able to adsorb CO_2 only, while N_2 is considered as inert;
- radial temperature and concentration gradients are neglected; all properties are homogeneous in the transverse section of the packed bed (plug-flow reactor assumption);
- adsorption kinetics follows a linear driving force (LDF) model, in which the adsorption driving force is as a linear function of the active component concentration in the gas phase [31];
- thermal capacity of the solid components is temperature independent;

- thermal capacity of the gas phase is described by a linear function of temperature, complying to the ideal gas law;
- heat exchange between the adsorption bed and the external environment occurs by natural convection; room temperature and external heat transfer coefficient are assumed constant over time and spatially uniform;
- pressure loss is evaluated in the condition of stationary flux, neglecting the influence of gravity.

Local mass, momentum and energy balances, written under the above simplification, are integrated by a time implicit finite volume discretization method, with a constant time-step. See the appendix section for further details.

3. Experimental results

3.1 Thermogravimetric results

The thermogravimetric results of CO_2 adsorption/desorption cycles in $NaG_{1.2}Z$ and zeolite Na13X are illustrated in Fig. 3, reported as relative weight change (Fig. 3a), obtained in isothermal conditions at T=35 °C, with constant flow of pure N_2 and CO_2/N_2 (y_{CO_2} = 0.20). The results of DSC analysis are also reported (Fig.3b), as obtained simultaneously. The insets display the last cycle of each series.

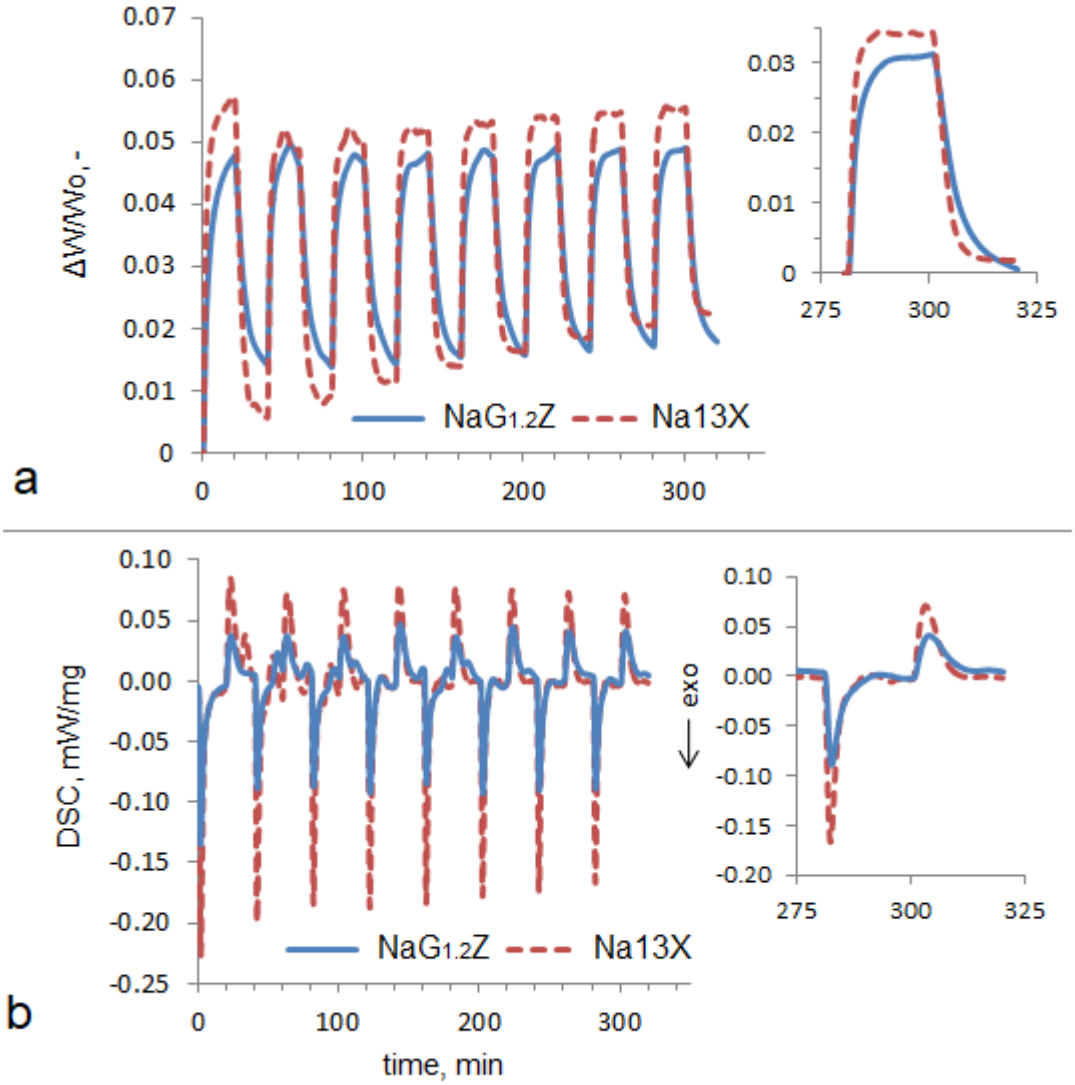

Figure 3. TG/DSC results of CO_2 adsorption and desorption cycles on $NaG_{1.2}Z$ and zeolite Na13X sorbents in isothermal conditions (35 °C) at atmospheric pressure and with y_{CO_2} =20%: (a) normalized weight change; (b) DSC curves. In the insets, the results obtained in the last adsorption/desorption cycle.

Interestingly, the relative weight changes during the last adsorption/desorption cycles show very similar values for the two sorbents, about 3.1% for $NaG_{1.2}Z$ and 3.4 % for Na13X, corresponding to a CO_2 capacity of 0.70 and 0.77 mmol/g, respectively. In this range of CO_2 partial pressure (0.2 atm), indeed, the adsorption properties of the two solid adsorbents have been found comparable even in static equilibrium adsorption tests [12], as it will be later discussed.

The comparison of adsorption and desorption branches reveals significantly different kinetics, as the regeneration step is slower than the adsorption step. As one can see, indeed, the $\Delta W/W_0$ signal is smoother in desorption and the DSC peak is broader and lower. Such an effect seems to be more relevant for the geopolymer based sorbent. Such a difference in the rate of adsorption and in that of desorption indicates the mass transport is partially hindered during the regeneration step, thus lowering the removal of CO_2 from the solid adsorbent, thus suggesting that mass transport effects at the particles boundary are significant, especially in the case of geopolymer/zeolite composite.

The analysis of the DSC signals (Fig. 3b) allowed the direct determination of CO_2 adsorption enthalpies, equal to -29.5 ± 2.0 and -39.5 ± 2.0 kJ/mol for $NaG_{1.2}Z$ and zeolite Na13X, respectively. The value measured on zeolite Na13X falls in the range typically reported for this material in the technical literature [13, 15], while the lower enthalpy for $NaG_{1.2}Z$ sample is due to the presence of zeolite Na4A (40 mol.%), having $\Delta\tilde{H}_{ads}$ of about 34 kJ/mol [16, 17], along with an amorphous phase (33 mol. %). Consequently, the adsorption enthalpy of the amorphous phase only may be estimated equal to about 16 kJ/mol on the basis of a simple additive effect.

3.2 Results of static sorption experiments

The results of CO_2 adsorption at different temperatures are reported in Figure 4, as they have been measured in static experiments by the pressure decay apparatus. The obtained values are indicative of the equilibrium CO_2 capacity of the solid adsorbent at a certain T and CO_2 partial pressure, ensuring sufficiently long adsorption time. As expected, CO_2 capacity decreases at increasing temperature, indicating a negative adsorption enthalpy.

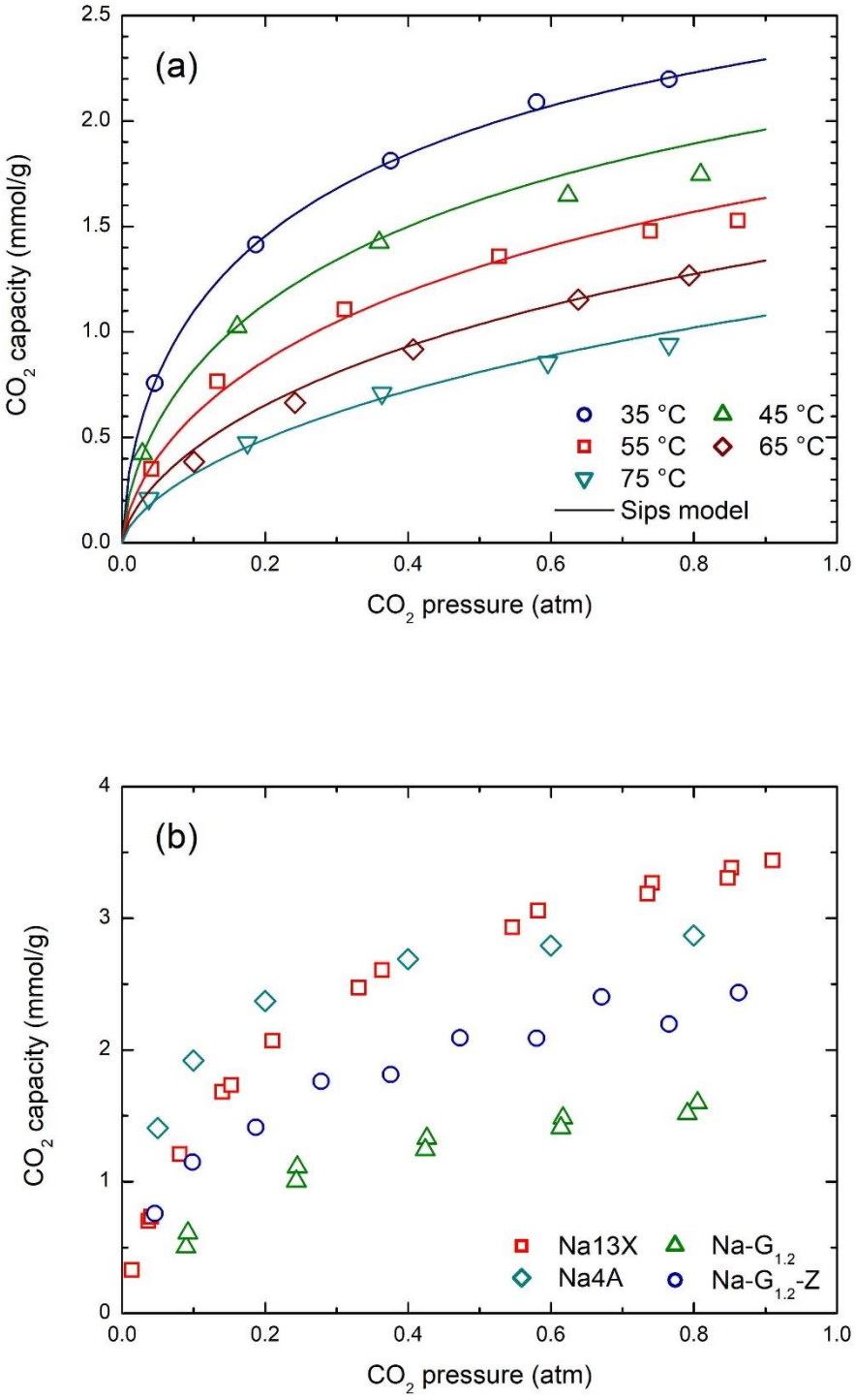

Figure 4. (a) CO_2 adsorption capacity of $NaG_{1.2}Z$ at different temperatures, measured by static equilibrium adsorption tests, together with the Sips model curves; and (b) comparison of the CO_2 capacity of $NaG_{1.2}$, $NaG_{1.2}Z$ and zeolite 13X [12] and that of Na4A [32] (T= 35°C).

The measured data allowed the determination of the Sips model parameters, able to describe the adsorption capacity at different temperature and pressures. The model curves are included in the plot in Figure 4a, while the parameters are listed in Table 2, after their values have been calculated from the best fitting of the experimental data.

Table 2. Sips model parameters obtained by the best fit of the experimental CO_2 adsorption data in geo/zeo composite NaG1.2Z at different temperatures (35-75 °C).

α	12.7 mol/kg
Θ	2.10 kJ/mol
Ω	1.26 10^{-8} atm
θ	-33.0 kJ/mol
s_1	2.0
s_2	0.0018 K^{-1}
s_R	0.50

Figure 4b compares the CO_2 capacity at 35 °C of the composite material of interest ($NaG_{1.2}Z$) with those of the neat Na-based geopolymer ($NaG_{1.2}$) and pure zeolite Na13X, used as filler in the composite of interest in this work. Relevantly, zeolite Na13X represents also the benchmark for carbon capture application. Furthermore, literature data of CO_2 capacity in zeolite Na4A, the crystalline phase formed during the geopolymerization reaction (see SEM micrograph in Figure 1c), is also included for the sake of comparison.

As one can see, the two pure zeolites Na13X and Na4A present the highest CO_2 capacity, although with different saturation points, as adsorption curve of the latter zeolite presents a plateau value at pressure higher than 0.5 atm. The geopolymer/zeolite composite NaG1.2Z shows very interesting performances, with a CO_2 capacity only slightly lower than that of neat Na13X in the relevant range for post combustion carbon capture (i.e. for CO_2 partial pressures from 0 to 0.20 atm).

Therefore, the composite material combines the peculiarities of the geopolymer matrix, able to shape self-supporting materials in different geometries using a low energy consolidation process in water [33, 34] with the good adsorption performances of the zeolite Na13X used as a filler. Furthermore the specific stoichiometry of the geopolymer matrix allows the formation of NaA [25] further boosting the CO_2 capacity, leading to an high selectivity towards N_2 that makes the composite an interesting candidate for post combustion carbon capture by adsorption process.

3.3 Results of dynamic experiments

Typical results of dynamic adsorption experiments in the composite solid sorbent $NaG_{1.2}Z$ are reported in Figure 5, which displays the time-behavior of the CO_2 molar fraction leaving the fixed bed (at the outlet section) for two different type of tests carried out: i) upon completion of adsorption, followed by regeneration (Fig. 5a), and ii) after achievement of breakthrough (set at a concentration threshold equal to 5% the feed CO_2 content), followed by regeneration step lasting 60 min (Fig. 5b). The first type of experiment allows the determination of the maximum equilibrium adsorption capacity in dynamic tests, while the second one resembles the real process conditions, with a reduced working capacity. All tests have been carried out at room temperature (T = 21 °C) after appropriate sample conditioning (at 130 °C for 60 min under continuous N_2 flux), and using a constant feed N_2 molar flow rate 30 NL/min, with 14.3% CO_2 molar fraction during adsorption.

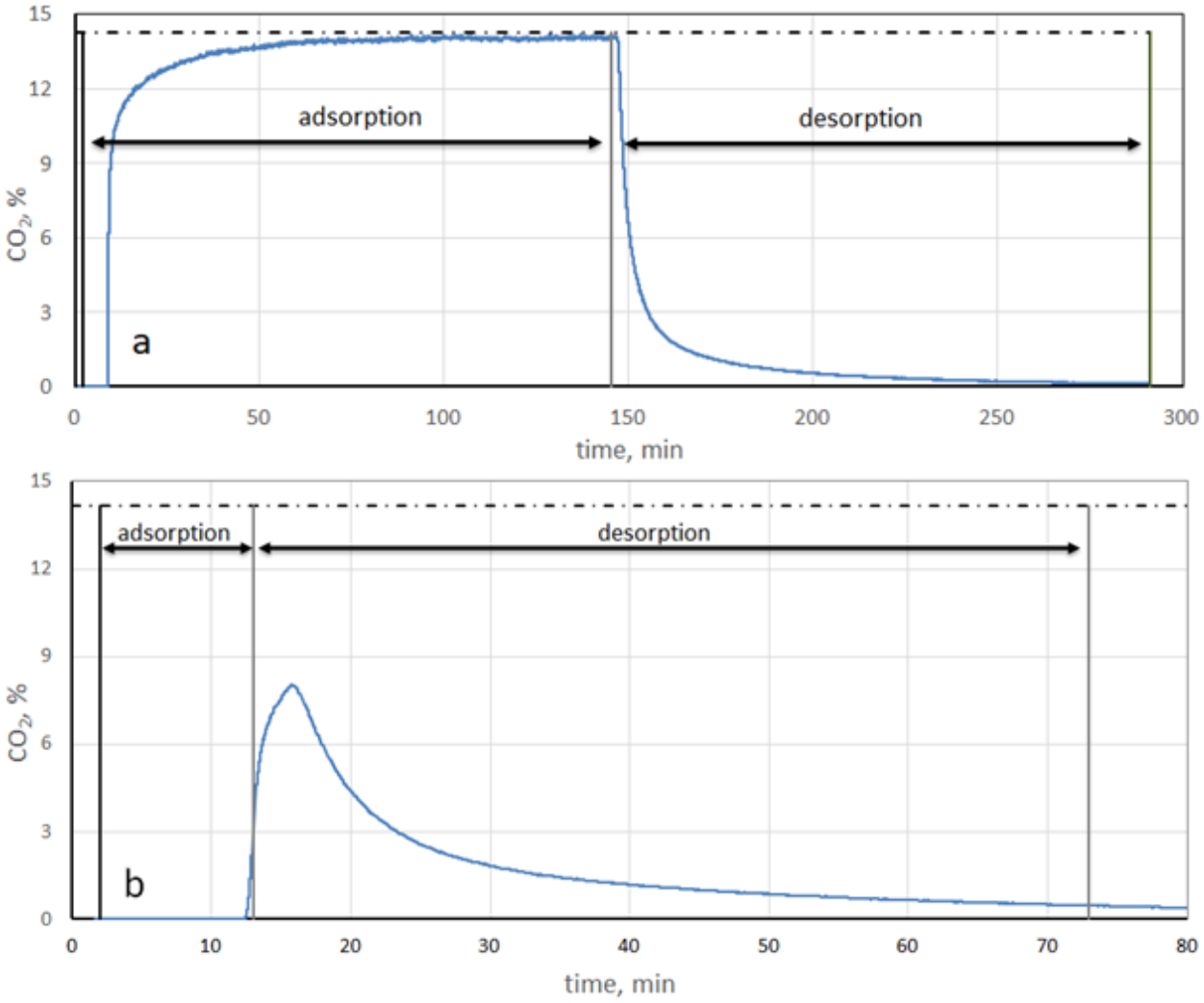

Figure 5. CO_2 outlet molar concentration in adsorption and desorption steps at room temperature (T_{des} = 21 °C), with CO_2 feed molar fraction $y^{in}_{CO_2}$ = 14.3 % (dashed lines): (a) complete adsorption/desorption test; (b) adsorption test stopped at breakthrough (5% of $y^{in}_{CO_2}$) and subsequent 60 min desorption segment ($NaG_{1.2}Z$)

As one can see, the complete adsorption occurred after about 140 min (Fig. 5a), where the CO_2 profile reaches a clear plateau. Conversely, the breakthrough time (corresponding to the achievement of CO_2 molar fraction 5 % x 14.3 % mol. = 0.0715 % mol. In the outlet section) in the second type of experiment has been observed at about 11 min (Fig. 5b). The vertical lines in the plots indicate the switch from adsorption to desorption steps ($t = t_0$, $t = t_0 + t_{ads}$ and $t = t_0+t_{ads}+t_{des}$). The adsorption curve obtained in the first type of experiment reveals that the adsorption process is basically completed within a few minutes only, and most of the remaining time is almost

ineffective (from about 30 to 150 min), as only a small amount of CO_2 is eventually captured by the sorbent. Conversely, in the second mode, a peak of CO_2 content is observed after the BT time, before a slower decay of the concentration profile (Fig. 5b). At the initial time of regeneration (by means of pure N_2 stream), and for few minutes, the CO_2 concentration in the outlet section of the adsorbent bed increases, as a consequence of the release of the adsorbate from the geopolymer/zeolite composite sorbent.

The comparison of the results obtained in the adsorption tests following the two procedures (complete vs. BT tests) indicates that in breakthrough mode one can achieve an adsorbed amount of CO_2 equal to about 50% of that in complete test, but in much shorter times (11 vs. 140 min).

The results of the complete dynamic adsorption tests are summarized in Table 3 as actual concentration of CO_2 in the solid phase (q_{CO_2}) at different feed CO_2 molar ratio ($y^{in}_{CO_2}$). Although the test temperature is rather different, the highest value 1.40 mmol/g is comparable with the measured one by static sorption tests (Fig. 4b) at T=35 °C.

Table 3. Results of complete dynamic adsorption tests at T=21 °C

$y^{in}_{CO_2}$, %	q_{CO_2}, mmol/g
5.0	0.67 ±0.09
7.5	0.92 ±0.10
14.3	1.20 ±0.08
19.3	1.40 ±0.11

The adsorption process, due to its exothermic nature, is accompanied by the release of energy while occurring. Indeed, appreciable thermal effects may be observed during adsorption and desorption steps, and the observed time behaviour of the temperature measured by the internal

probe within the sorbent bed is reported in Figure 6, together with the outlet CO_2 molar fraction. Noteworthy, the reported behaviour has been obtained with no external control of the temperature. An increase in temperature is indeed very visible at early times of adsorption with ΔT larger than 10 °C, and the peak is observed shortly after the BT time, as the adsorption rate is maximum in those conditions. After that, the temperature slowly decreases, as the adsorption rate is decreasing due to the progressive saturation of the bed.

Negative deviations of the temperature have been obtained during desorption, but only few °C differences have been detected, due to the slower rate already observed in TG tests (Fig. 3).

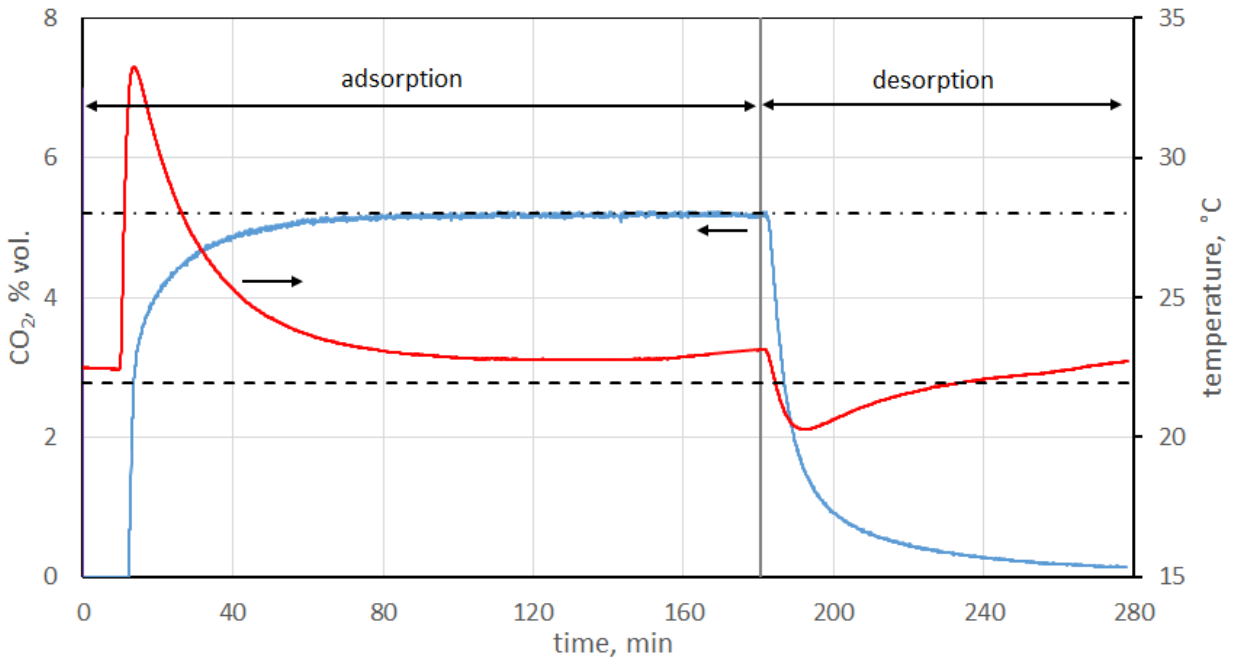

Figure 6. CO_2 molar concentration and internal bed temperature profiles ($NaG_{1.2}Z$, $y_{CO_2}^{in}$ = 5.2 mol. % dashed-dotted line; T_∞= 22 °C dashed line)

It is worth to note that the increase in temperature depresses the actual adsorption capacity, due to the exothermic nature of the process (see Fig. 4a), and thus the maximum adsorption capacity

in the dynamic experiments is reached once steady conditions have been attained, i.e. when the temperature has dropped back to room conditions. Same considerations apply for desorption.

Figure 7 displays the CO_2 apparent adsorption capacity measured at the breakthrough and the corresponding peak temperature measured within the packed bed reported versus the feed CO_2 content. Indeed, the larger the adsorbed CO_2, the higher the peak temperature. The maximum temperature increase has been measured as high as 20 °C at $y_{CO_2}^{in}$ = 19 %, corresponding to a CO_2 capacity of about 0.7 mmol/g.

Interestingly, the large temperature increase associated to higher CO_2 molar fraction in feed depresses adsorption more significantly than at lower values, so the resulting capacity at the BT deviates more appreciably from the that obtained in complete adsorption tests (see Table 3).

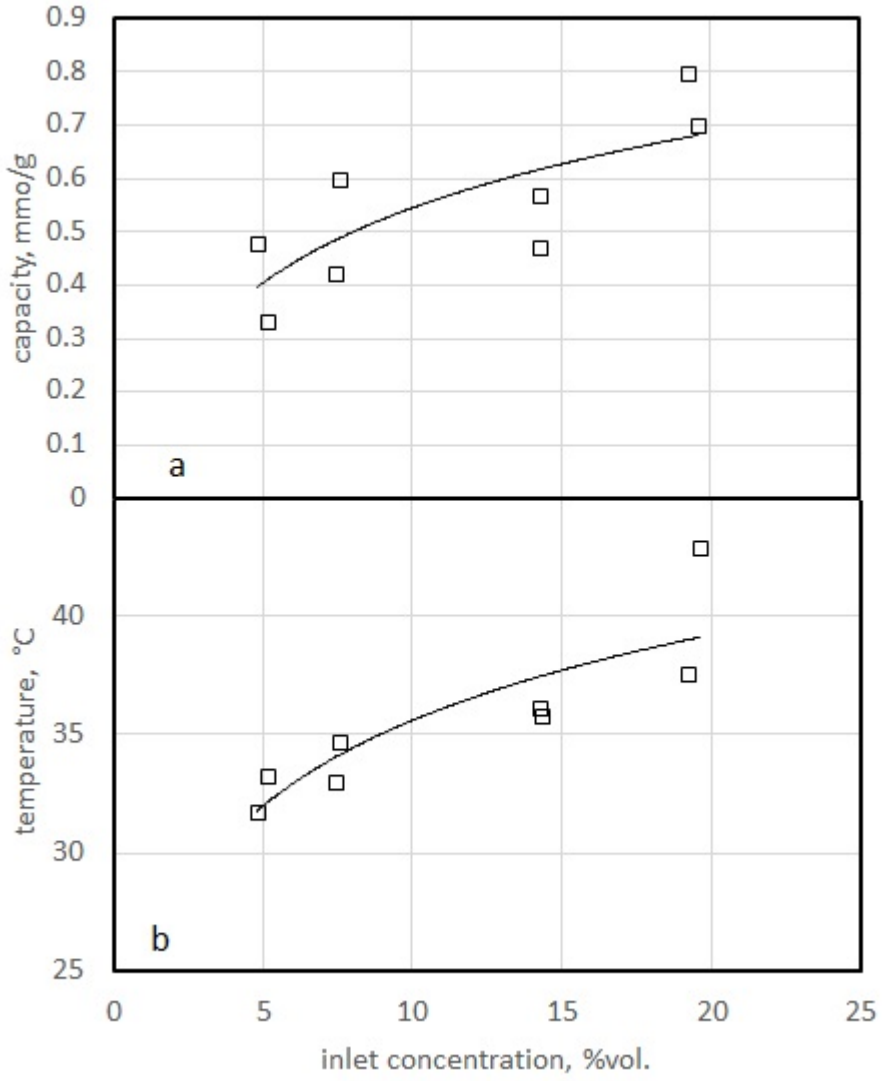

Figure 7. (a) adsorption capacity at breakthrough and (b) peak temperature during adsorption versus feed CO_2 molar fraction (T_{des}=21°C). ($NaG_{1.2}Z$, $y_{CO_2}^{in}$ = 14% mol.)

The mutual interaction between CO_2 adsorption and temperature fluctuation is even more apparent in Figure 8, which shows the adsorption rate (i.e. $d\chi/dt$), determined from experimental data by the numerical derivation of Eq. 6 and 7, and the temperature in the sorbent bed versus the adsorption degree (χ) for a test carried out at room conditions. In isothermal condition the adsorption rate is dependent on various factors, such as kinetics of vacant active site interaction, inter/intra particle gas diffusion, resistance in the film surrounding the adsorbent particle [35]. As one can see, the adsorption rate remains constant (equal to its maximum value $7.7 \cdot 10^{-4}$ s^{-1}) for χ

up to 0.3, and it markedly decreases in the narrow window [0.3, 0.4], afterwards the adsorption rate approaches asymptotically zero because of the depletion of active sites. The marked decline in the adsorption rate occurs shortly after the temperature peak (Fig. 8), suggesting that the sorbent temperature increase further depresses the overall kinetics, because the higher the sorbent temperature, the lower the CO_2 capacity (Fig. 4) and, consequently, the smaller is the driving force of adsorption.

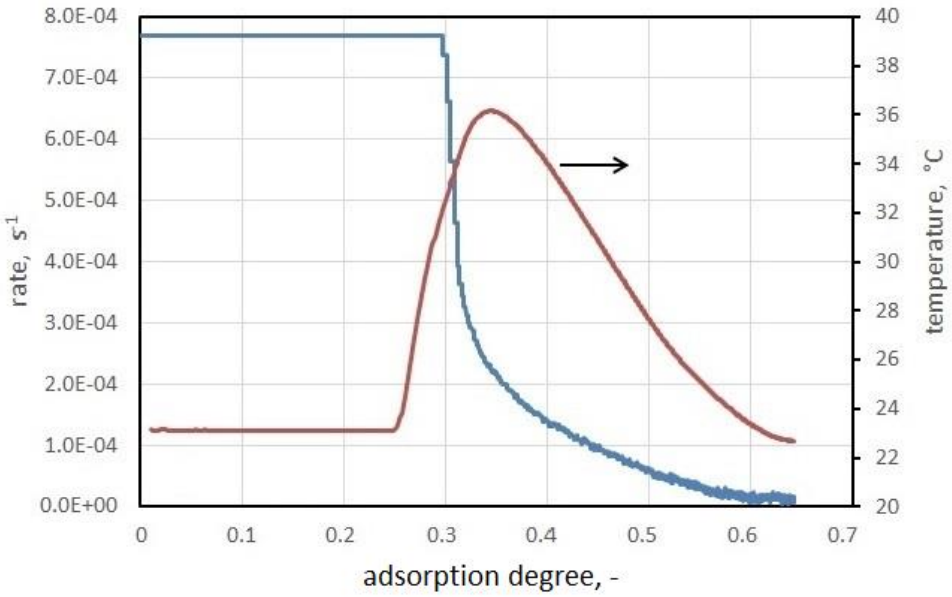

Figure 8. Adsorption rate and fixed bed sorbent temperature versus adsorption degree at room temperature ($NaG_{1.2}Z$, $y^{in}_{CO_2}$ = 14% mol.).

The results reported above (Figs. 6-8) point out the relevance of sorbent temperature during the process. Therefore, CO_2 desorption and thus its mass transport from the solid to the gas phase may be guided not only by the different partial pressure (pure N_2 is used to this aim) but also by increasing the temperature in the regeneration step in a mixed PSA/TSA strategy.

Figure 9 shows the effect of the heating during desorption segment for three consecutive cycles carried out up to the breakthrough point. The electric heater is activated immediately after the adsorption segment and the temperature is maintained higher than room conditions for 60 min

(T_{des}=130±3 °C in Fig. 9b) for about 60 min. Afterwards, the sorbent bed is cooled down to room temperature before starting next adsorption stage, to prevent a depression of the sorbent capacity. During all of these operations, the inert N_2 flowrate fed to the adsorption bed was constant.

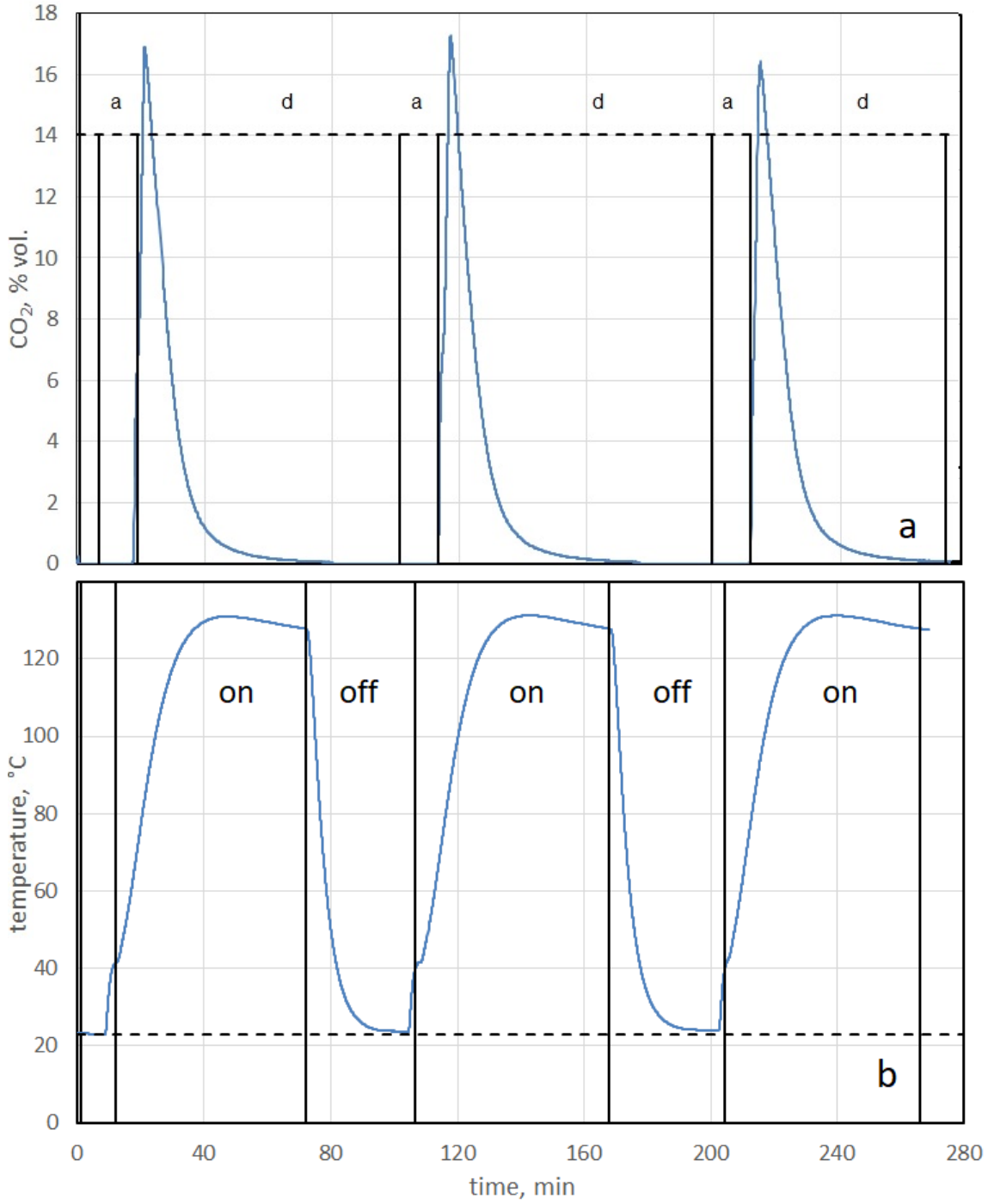

Figure 9. Profiles of (a) CO_2 concentration ($y^{in}_{CO_2}$ = 14.0 % mol. dashed line) and (b) temperature at the outlet section of the adsorption bed during a breakthrough test of adsorption and regeneration at higher temperature, room temperature (T_∞=23 °C) is indicated as a dashed line. ($NaG_{1.2}Z$, $y^{in}_{CO_2}$ = 14% mol.) a: adsorption; d: desorption; on: heater on; off: heater off

As one can see, the consecutive repeated cycles show basically the same behavior both for outlet CO_2 content (Fig. 9a) and bed temperature (Fig. 9b), indicating of good repeatability of such

method. Interestingly, the CO_2 molar fraction exhibits a peak higher than the feed concentration shortly after switching on the heater at the beginning of regeneration stage; then, it quickly declines to zero. A certain time has been then devoted to cool down the adsorption bed to room condition before the following adsorption step. In a real TSA-PSA process, the choice of both T_{ads} and T_{des} has to be optimized in order to maximize the rate of captured CO_2 over time.

The regeneration temperature affects significantly not only the CO_2 desorption rate, but also the CO_2 working capacity, which may be lowered by an incomplete sorbate release. The resulting capacity during consecutive cycles of the same duration (BT time during adsorption plus 60 min desorption) as function of regeneration temperature is reported in Figure 10. As one can see, the first cycle, performed upon complete regeneration of the sorbent, shows the largest CO_2 capacity, while it is soon deteriorated, in the second cycle, if the desorption is carried out at room temperature, which in turn would require much longer time. That is indicated in Figure 10b, which displays the capacity of the second and third cycle versus the desorption temperature. Relevantly, the capacity has been increased appreciably carrying out the regeneration stage at 88 °C or higher values, reaching an asymptotic trend at high temperatures. Such result indicates that the temperature swing strategy coupled with partial pressure swing is significantly more effective than changing only P or T during desorption. However, an excessive increase in T_{des} would require larger amount of heat and longer times for cooling down the sorbent bed to room temperature, decreasing the process efficiency.

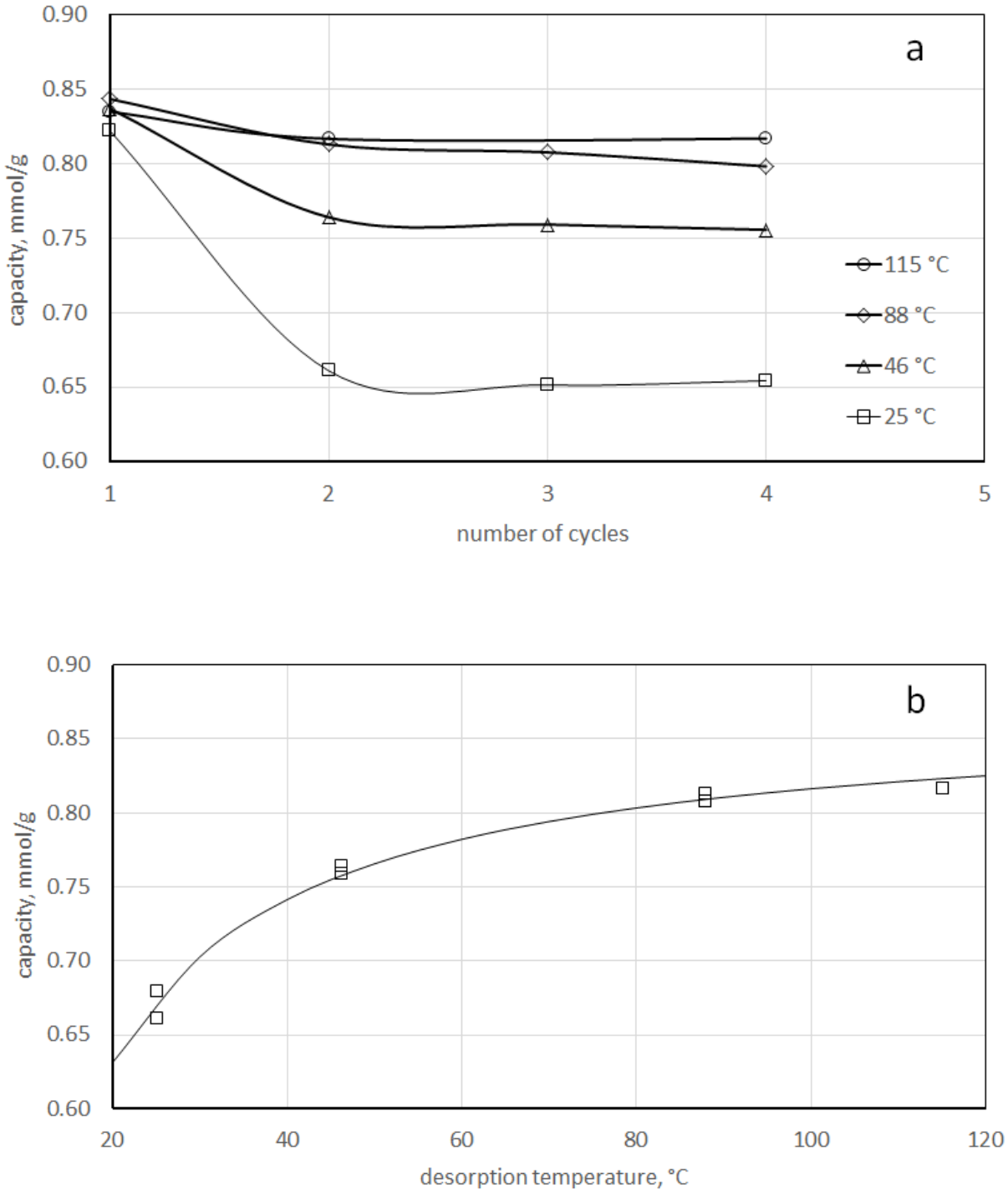

Figure 10. CO_2 working capacity at breakthrough versus (a) cycle number; (b) desorption temperature ($NaG_{1.2}Z$, $y_{CO_2}^{in}$ = 14% mol.)

Model results

The values of the parameters used for model calculation are summarized in Table 4. The external heat transfer coefficient was set to 15 W/m^2K, as estimated for heat transfer by natural convection mechanism. The temperature for evaluation of properties (T_{ref}) has been chosen as average value taking into account the temperature peaks. All other relevant thermodynamic properties for solid and gaseous species have been taken from the available literature. The model is able to predict the time dependent profiles along the adsorption bed axis of CO_2 concentration and temperature. For the sake of shortness, the computed values at outlet section of the bed only have been taken into consideration.

Table 4. Material and transport properties used in the model.

External heat transfer coefficient, $W/(m^2 K)$	15
T_{ref}, °C	35
Mass transfer coefficient, h^{-1}	200 [36]
Gas diffusion coefficient at T_{ref}, mm^2/s	17.3 [37]
Solid specific heat, J/(g K)	0.96 [33]
Gas phase viscosity, cP	$1.88\ 10^{-2}$ [38]
CO_2 specific heat, J/(mol K)	37.74 [38]
N_2 specific heat, J/(mol K)	29.13 [38]

The predicted profiles of CO_2 concentration and bed temperature at outlet section of the bed are shown in Figures 11 and 12, for the case of inlet CO_2 concentration equal to 19% mol. As one can see, the comparison is qualitatively good in both adsorption and desorption stages, in term of kinetics of variation for CO_2 concentration and temperature at the outlet section of the bed.

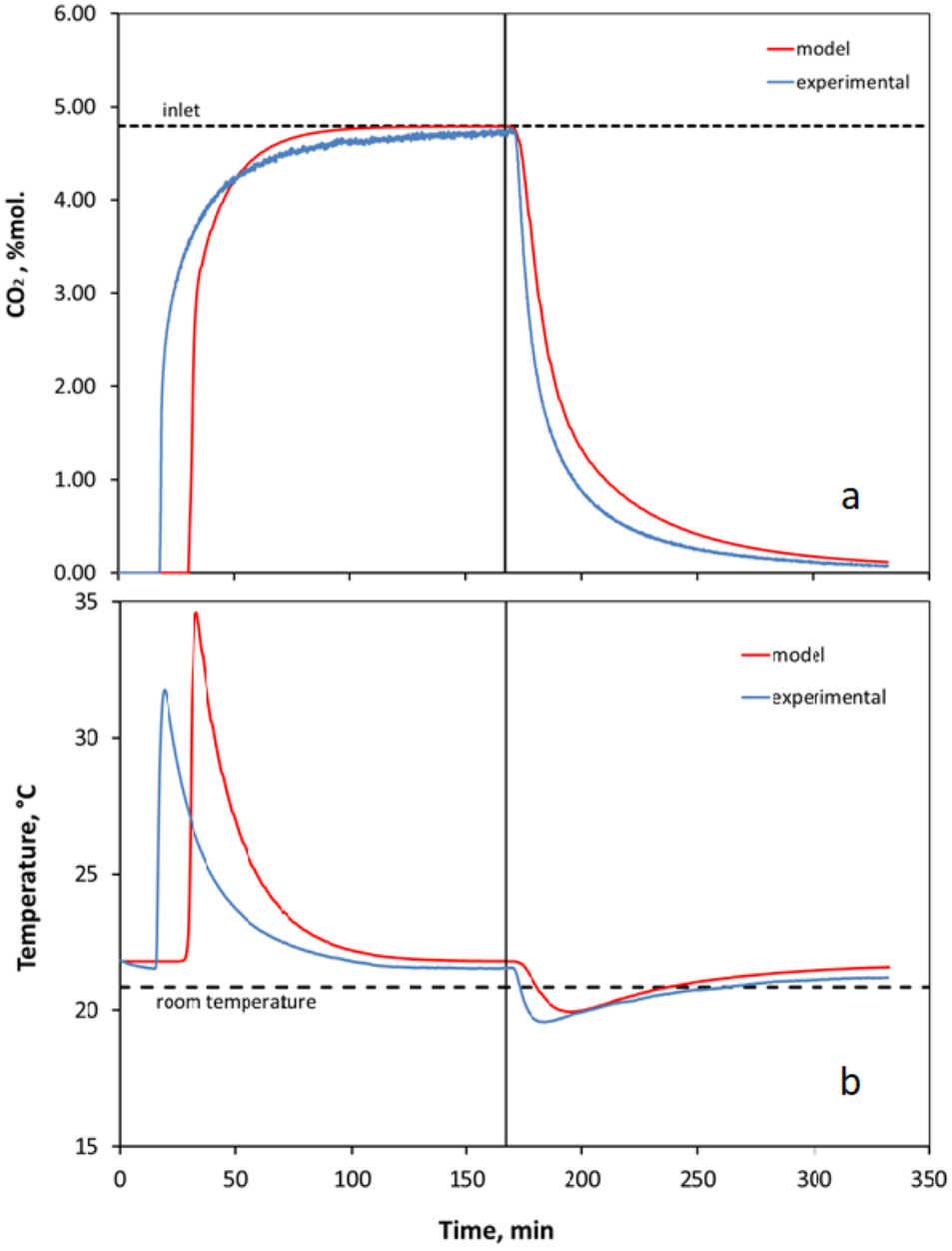

Figure 11. Comparison of experimental and model CO_2 molar concentration (a) and temperature (b) at outlet section of the bed for complete adsorption tests at inlet CO_2 concentration of 19%. The vertical line indicates the switch time from adsorption to desorption step. The model curve was evaluated assuming completely regenerated bed as initial condition.

On the other hand, breakthrough time predicted by the model according to the data in Fig.11 is significantly higher than the corresponding value from the experimental analysis and an overestimation finally results for the effective capacity of the sorption bed. In fact, several different origin could be considered, in principles, for the latter discrepancy between experimental

results in dynamic sorption process and pertinent model prediction based on thermodynamic data retrieved from static sorption experiments. In the present analysis, however, an interpretation of the experimental data for breakthrough time is just offered by means of the assumption the regeneration process for the adsorption bed before the sorption step is not complete and a residual non-zero fugacity for CO_2 at the process temperature need to be considered as initial condition in the adsorption bed.

In Fig. 12 the comparison is offered between experimental results and model predictions pertinent the same run considered in Fig.11, for the case in which the initial CO_2 fugacity in the bed is treated as an adjustable parameter and set at the value of 3 mbar.

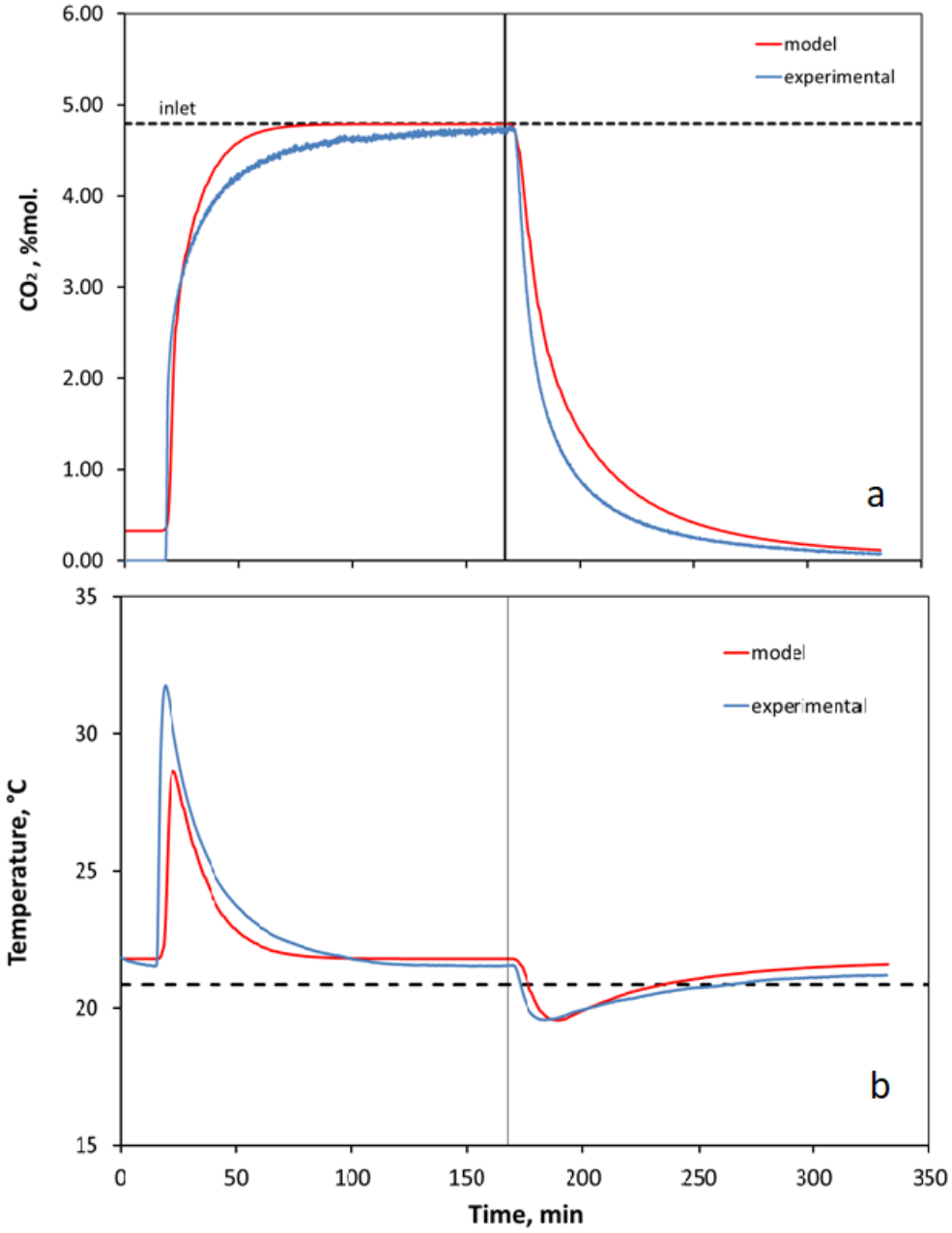

Figure 12. Comparison of experimental and model CO_2 molar concentration (a) and temperature (b) at outlet section of the bed for complete adsorption tests at inlet CO_2 concentration of 19%.. The vertical line indicates the switch time from adsorption to desorption step. The model curve was evaluated assuming the residual CO_2 fugacity in the bed is 3 mbar as initial condition for the process.

The assumption of incomplete regeneration of the bed before the adsorption run allows for an accurate representation (Fig. 12a) of breakthrough time for CO_2 concentration, as well as an acceptable description is also offered by the model for the temperature variation at the outlet section of the bed (Fig. 12b).

It is finally observed that the same assumption (initial solute fugacity in the bed equal to 3 mbar) also allows for a good representation of experimental data measured for the case of different CO_2 concentration in the feed stream.

The accuracy of the model in the description of the experimental results is reported in Table 5 as average standard deviation of CO_2 concentration and temperature for the four simulated experiments of adsorption and desorption (see Table 3). For each cell, the first value is pertinent to complete regeneration, whilst the second one to 3 mbar fugacity regeneration. In all cases a substantial decrease of the standard deviation can be noted, confirming the better accuracy of the model shown in Fig. 12.

Table 5. Standard deviations of output concentration and temperature between model and experimental results

CO_2 concentration in the feed % mol.	Standard deviation of CO_2 concentration % mol.	Standard deviation of temperature °C
5.2	1.1 / 0.70	3.1 / 1.6
7.6	0.74 / 0.42	1.9 / 1.2
14.0	2.0 / 1.4	2.2 / 1.6
20.0	1.6 / 0.77	3.5 / 2.8

In order to analyse the effect of heat transfer coefficient *h* in the process and to discuss the residual discrepancy between modelling and experimental results, the value of *h* has been finally adjusted to optimize the representation of temperature rise in adsorption run with entrance CO_2 concentration equal to 19.2% mol. Results for the complete adsorption/desorption test are reported in Fig.13. By reducing the external heat transfer coefficient from 15 down to 9.0 W/m^{2}K, the temperature rise in adsorption step is satisfactorily represented, while the prediction largely overestimate the decrease of temperature in the desorption step. The latter result can be considered as a limit of the linear driving force approach (LDF) used in the model [31], which is not able to capture the difference in the rate of sorption and desorption step the experimental data

exhibits. In fact, the results from measurements for both CO_2 concentration (in term of characteristic time of concentration variation) and temperature (in term of temperature peak) at the outlet section in the bed confirm the effective resistance to mass transport in the bed during desorption process is higher than sorption step.

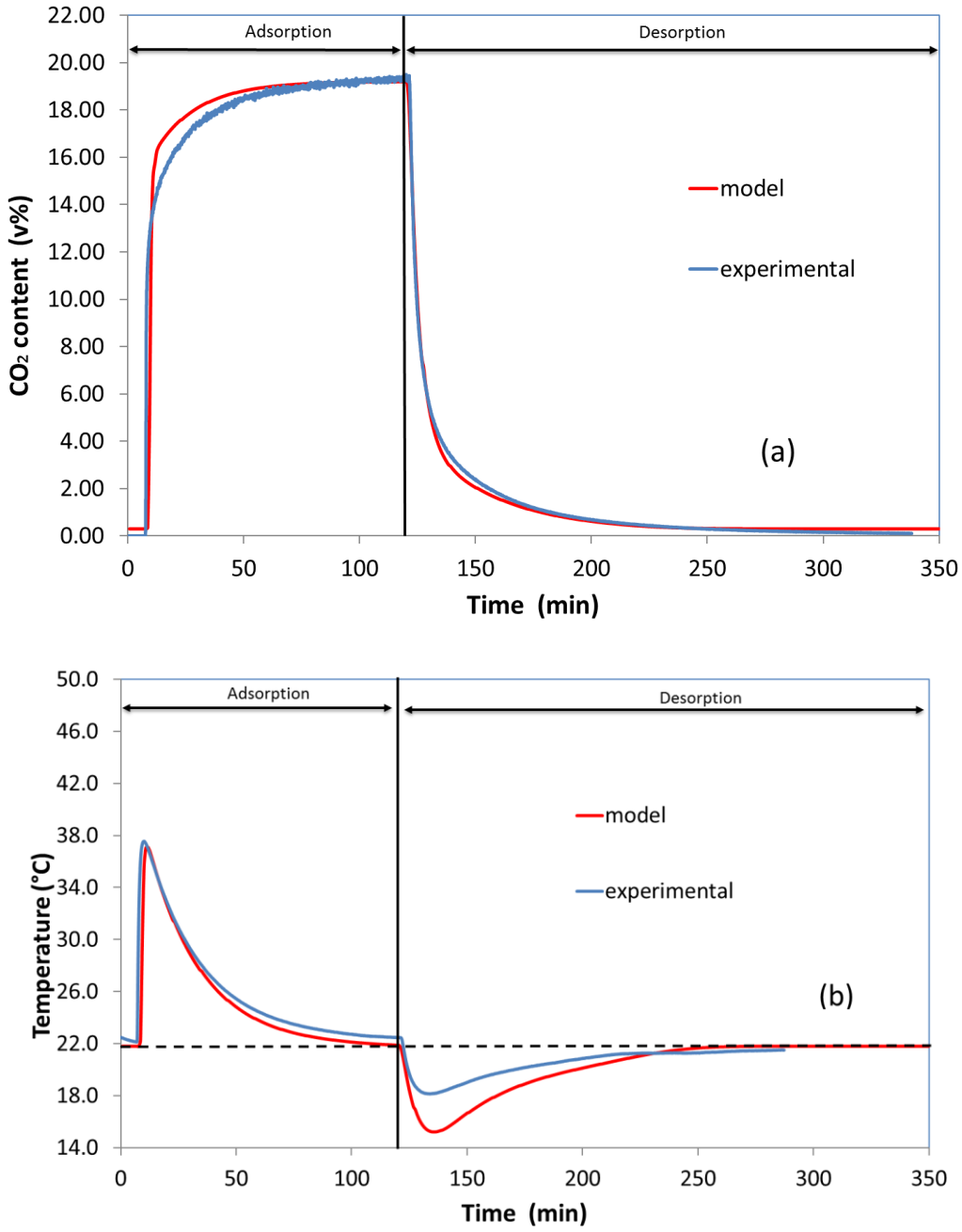

Figure 13. Comparison of experimental and model CO_2 molar concentration (a) and temperature (b) at outlet section of the bed for complete adsorption test at inlet CO_2 concentration of 19% mol. The vertical line indicates the switch time from adsorption to desorption step. The model curve

was evaluated assuming the residual CO_2 fugacity in the bed is 3 mbar as initial condition for the process and the heat transfer coefficient h = 9.0 W/m^{2}K.

Also the value of heat transfer coefficient retrieved from the best fit of temperature rise in adsorption test for the case at maximum CO_2 concentration in the inlet stream (h = 9.0 W/m^{2}K) has been successfully used to represent the experimental data measured for runs at lower CO_2 content. As an example of these results, Fig.14 shows the comparison between experimental data and modelling calculations for the case of inlet stream at lowest CO_2 concentration in the range examined (4.8 % mol). Indeed, it can be appreciated from the plot in Fig.14 that assuming the initial CO_2 fugacity in the adsorption bed is equal to 3 mbar the breakthrough time is correctly predicted by the model. In addition to that, accounting for a value of heat transfer coefficient in the external phase equal to 9.0 W/m^{2}K, the model correctly predicts the temperature rise in the adsorption step for the same experimental run, while it overestimate the thermal effect in the desorption step, parallel to the results for the run at higher concentration.

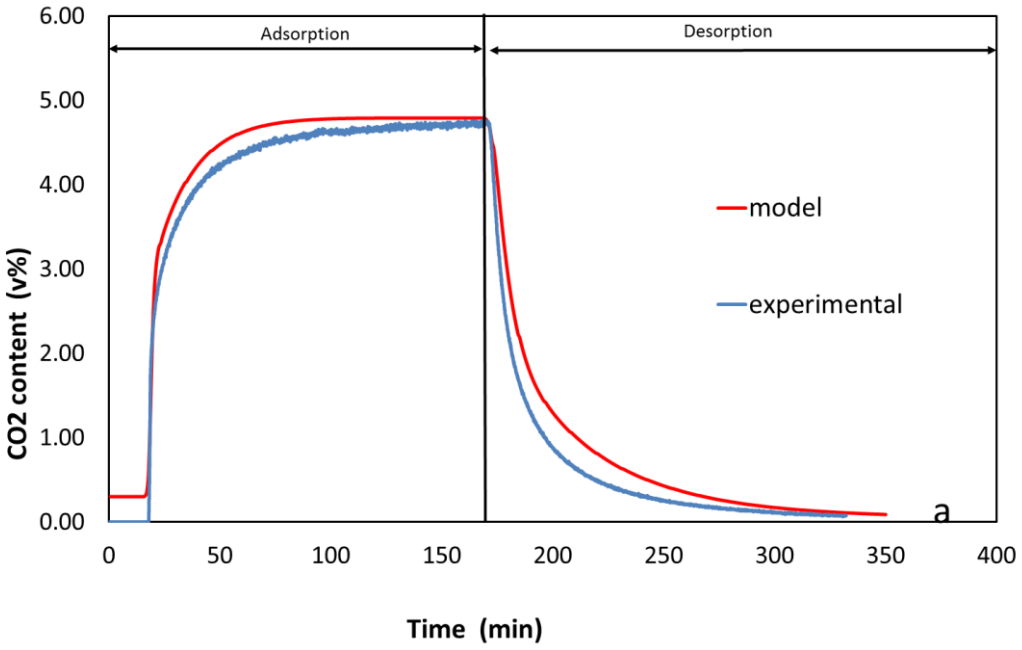

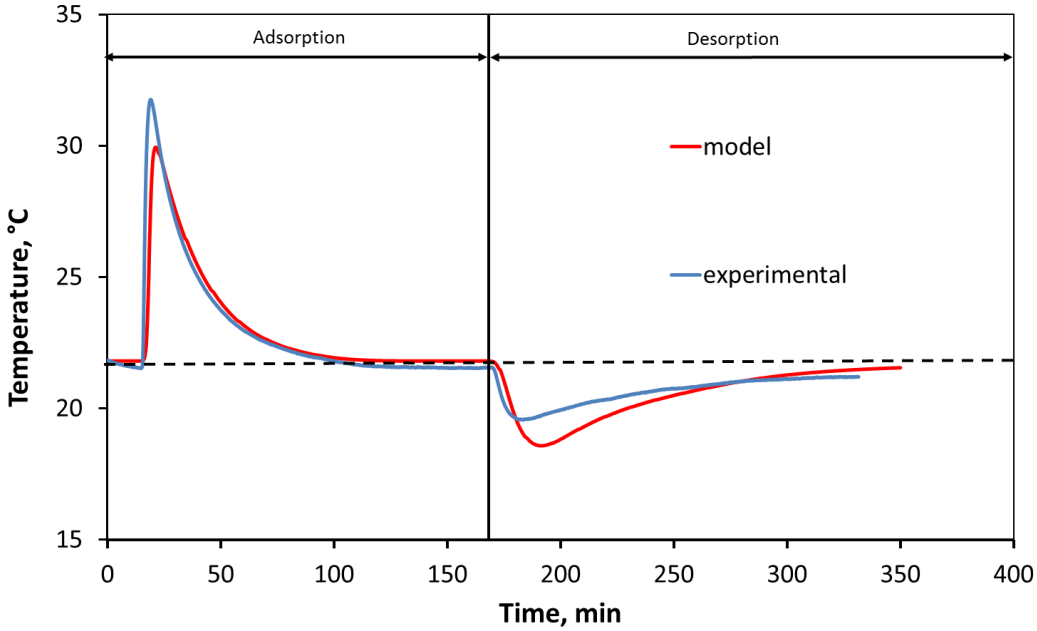

Figure 14. Comparison of experimental and model CO_2 molar concentration (a) and temperature (b) at outlet section of the bed for complete adsorption tests at inlet CO_2 concentration of 4.8%. The vertical line indicates the switch time from adsorption to desorption step. The model curve was evaluated assuming the residual CO_2 fugacity in the bed is 3 mbar as initial condition for the process and the heat transfer coefficient h = 9.0 W/m^{2}K.

Conclusions

The CO_2 adsorption/desorption in a geopolymer-zeolite composite has been investigated with particular focus on the associated thermal effects in TG, static and dynamic tests. Firstly, the adsorption enthalpy of the sorbent was determined in TG apparatus and resulted equal to -29.5 ± 2.0 mmol/g.

The static tests provided the complete set of equilibrium adsorption curves at changing temperature from 35 to 75 °C, as preparatory step to dynamic tests. The dynamic tests with complete saturation of the bed provided results in terms of CO_2 capacity very close to those of static experiments. Conversely, the sorbent capacity at breakthrough (i.e. 5% of the inlet CO_2 concentration) was always a substantially high fraction (40-60%) of the overall capacity from static tests, making less effective the further adsorption upon breakthrough time in a strategy of process optimization. The temperature peak during adsorption (up to 20 °C) was dependent on the CO_2 concentration in the feeding stream and resulted in a lowered overall adsorption/desorption rate due to the effect on the driving force of the process.

The thermal effect in adsorption/desorption can be exploited for the process optimization in particular by coupling the pressure swing operation with a superimposed temperature increase during desorption, as clearly demonstrated by specific tests carried out with external heating of the adsorption bed. In this respect, the thermal properties of the sorbent (e.g. specific heat and conductivity) are likely to play a dominant role.

The experimental results were compared with the outputs of a 1D numerical model of adsorption/desorption in a fixed bed of sorbent, able to predict the associated thermal effects. The use of the model allows to discuss the experimental results and specifically to represent the impact of the regeneration efficiency and to retrieve the effective value of the heat transfer coefficient. A confirmation of the corresponding values estimated from the best fit of

experimental results at the highest inlet concentration for CO_2 was given through the direct comparison with experimental data for the tests performed at lower CO_2 concentration. Overall, the comparison was good, opening the possibility to apply the novel developed model for process simulation and optimization.

Nomenclature

C	overall molar concentration, mol/m^3
$\tilde{C}$	molar heat capacity, J/(mol K)
D	mass transfer axial dispersion coefficient, mm^2/s
D_m	molecular mass diffusivity in the gas phase, mm^2/s
d_p	mean particle diameter of the sorbent, mm
f_{CO_2}	CO_2 fugacity, Pa
F	mass flowrate, kg/h
h	external heat transfer coefficient, W/(m^2 K)
K	heat transfer axial dispersion coefficient W/(m^2 K)
k_s	global mass transfer coefficient, 1/s
L	adsorption bed length, cm
m_s	sorbent mass, g
n	molar flux density of the gas, mol/(s m^2)
p	pressure, bar
q_{CO_2}	concentration of active component in the solid phase, mol/kg or mmol/g
$\dot{n}$	volumetric flow rate, mol/s or NL/s
q^*	equilibrium concentration of active component in the solid phase, mol/kg
R	universal gas constant, J/(mol K)
R_p	radius of the adsorption bed, m
s_1	parameter of the Sips equation, -
s_2	parameter of the Sips equation, 1/K
s_R	parameter of the Sips equation, -
T	temperature, K

t time, s

t_0 starting time for the adsorption step in the dynamic sorption experiment, s

t_{ads} duration of the adsorption step in the dynamic sorption experiment, s

t_{des} duration of the desorption step in the dynamic sorption experiment, s

V volume, m^3

y_{CO_2} molar fraction of CO_2 in the gas phase, -

Subscripts

ads adsorption

b bed

des desorption

g gas

in inlet value

out outlet value

s solid

t total

∞ room conditions

Greeks symbols

α parameter of the Sips equation, mol/kg

$\Delta\tilde{H}_{ads}$ molar adsorption enthalpy, kJ/mol

ε void fraction, -

Θ parameter of the Sips equation, kJ/mol

θ	parameter of the Sips equation, kJ/mol
χ	adsorption/desorption degree, -
μ	gas phase viscosity, cP
ρ	density, g/cm^3
σ	compressive strength, MPa
Ω	parameter of the Sips equation, atm^{-1}

Appendix

The model solves numerically the full set of mass (Eq. A1), species (Eq. A2 and A3), energy (Eq. A4) and momentum (Eq. A5) balance equations, in the domain $(0 \le t; 0 \le z \le L)$, where L is the length of the packed bed, while r is its radius. The packed bed contains solid adsorbent particles of diameter d_p and the resulting total and bed void fractions are ε_t and ε_b.

$$\varepsilon_t \frac{\partial c}{\partial t} + \frac{\partial n}{\partial z} + \rho_b \frac{\partial q_{CO_2}}{\partial t} = 0 \quad \text{(A1)}$$

$$\varepsilon_t \frac{\partial \left(c\, y_{CO_2} \right)}{\partial t} + \frac{\partial \left(n\, y_{CO_2} \right)}{\partial z} + \rho_b \frac{\partial q_{CO_2}}{\partial t} - \varepsilon_b \frac{\partial}{\partial z}\left(cD \frac{\partial y_{CO_2}}{\partial z} \right) = 0 \quad \text{(A2)}$$

$$\frac{\partial q_{CO_2}}{\partial t} + k_s \left(q_{CO_2} - q^*_{CO_2} \right) = 0 \quad \text{(A3)}$$

$$\left[\varepsilon_t \tilde{C}_g c + \rho_b \left(\tilde{C}_s + q_{CO_2} C^{ads}_{CO_2} \right) \right] \frac{\partial T}{\partial t} + n \tilde{C}_g \frac{\partial T}{\partial z} - \rho_b \Delta \tilde{H}_{ads} \frac{\partial q_{CO_2}}{\partial t} - \varepsilon_b \frac{\partial}{\partial z}\left(K_g \frac{\partial T}{\partial z} \right) + \frac{2}{R_p} h \left(T_\infty - T \right) = 0 \quad \text{(A4)}$$

$$\frac{\partial p}{\partial z} + \left[1.75 n + \frac{150 \mu \left(1 - \varepsilon_b \right)}{d_p} \right] \left(\frac{1 - \varepsilon_b}{\varepsilon_b^3\, d_p} \right) \frac{n}{c} = 0 \quad \text{(A5)}$$

where T and p are temperature and pressure in the sorbent bed, y_{CO_2} is the fraction of active component in the gas phase, n is the molar flux density of the gas in the axial direction and q_{CO_2} is the concentration of active component adsorbed in the solid (q^* is the corresponding CO_2 capacity). Gas phase concentration c and CO_2 fugacity f_{CO_2} (for Sips model) are calculated by Peng-Robinson equation of state.

The gaseous phase heat capacity (C_g) is assumed linearly dependent on temperature and composition, while a constant value is considered for the viscosity of the gaseous phase (μ), while the axial dispersion coefficients for mass transfer (D) and heat transfer (K_g) are calculated as follows:

$$D = \frac{K_g}{C_g} = 0.7D_m + 0.5\frac{d_p n}{c\,\varepsilon} \quad \text{(A6)}$$

where D_m is the molecular mass diffusivity.

The initial conditions are $p=p^0$ and $T=T^0$, assumed constant over the whole length, while the initial quantity of active component adsorbed, is calculated by the model from the input of the regeneration conditions (temperature, pressure and active component concentration in the regeneration feed). As boundary conditions the Eqs. A7-A9 apply at z=0 (in) and z=L (out).

$$z = 0 \;\Rightarrow\; y_{CO_2} = y_{CO_2}^{(in)}(t);\quad T = T^{(in)}(t);\quad n = \frac{\dot{V}_{CO_2}^{in} + \dot{V}_{N_2}^{in}}{\pi r^2}\frac{p}{RT} \quad \text{(A7)}$$

$$z = L \;\Rightarrow\; \frac{\partial y_{CO_2}}{\partial z} = \frac{\partial T}{\partial z} = 0;\quad p = p^{(out)}(t) \quad \text{(A8)}$$

$$p^0 = p^{(out)}(t=0) \quad \text{(A9)}$$

The model solves the differential equations through a time implicit finite volume discretization method [39], in which a grid of 100 equally spaces grid points are identified along the 1D domain (z axis) and a constant time-step is used, iterating for pressure, concentration and temperature profiles in three nested loops.

References

[1] M. Younas, M. Sohail, L.K. Leong, M.J. Bashir, S. Sumathi, Feasibility of CO2 adsorption by solid adsorbents: a review on low-temperature systems, International Journal of Environmental Science and Technology 13 (2016) 1839-1860.

[2] R. Ben-Mansour, M.A. Habib, O.E. Bamidele, M. Basha, N.A.A. Qasem, A. Peedikakkal, T. Laoui, M. Ali, Carbon capture by physical adsorption: Materials, experimental investigations and numerical modeling and simulations – A review, Applied Energy 161 (2016) 225-255.

[3] A. Gabelman, Adsorption Basics: Part 1, Chemical Engineering Progress, July (2017) 48-53.

[4] K.N. Gupta, R. Kumar, Kinetic modeling and optimization of fraction of bed utilized for the gaseous phase removal of toluene in fixed bed adsorption column: Response surface methodology, Separation Science and Technology 55 (2020) 1062-1077.

[5] D. Kunii, O. Levenspiel, CHAPTER 2 - Industrial Applications of Fluidized Beds, Fluidization Engineering (Second Edition), Butterworth-Heinemann, Boston, 1991, pp. 15-59.

[6] M.G. Plaza, S. García, F. Rubiera, J.J. Pis, C. Pevida, Post-combustion CO2 capture with a commercial activated carbon: Comparison of different regeneration strategies, Chemical Engineering Journal 163 (2010) 41-47.

[7] K.S. Walton, M.B. Abney, M. Douglas LeVan, CO2 adsorption in Y and X zeolites modified by alkali metal cation exchange, Microporous and Mesoporous Materials 91 (2006) 78-84.

[8] P. Ammendola, F. Raganati, C. R., F. Miccio, Thermodynamic and Kinetic Characterization of Yellow Tuff for CO2 Adsorption, Chemical Engineering Transactions 74 (2019) 1207-1212.

[9] A. Trewin, A.I. Cooper, Porous Organic Polymers: Distinction from Disorder?, Angewandte Chemie International Edition 49 (2010) 1533-1535.

[10] V. Gargiulo, M. Alfè, F. Raganati, L. Lisi, R. Chirone, P. Ammendola, BTC-based metal-organic frameworks: Correlation between relevant structural features and CO2 adsorption performances, Fuel 222 (2018) 319-326.

[11] M. Minelli, V. Medri, E. Papa, F. Miccio, E. Landi, F. Doghieri, Geopolymers as solid adsorbent for CO2 capture, Chemical Engineering Science 148 (2016) 267-274.

[12] M. Minelli, E. Papa, V. Medri, F. Miccio, P. Benito, F. Doghieri, E. Landi, Characterization of novel geopolymer – Zeolite composites as solid adsorbents for CO2 capture, Chemical Engineering Journal 341 (2018) 505-515.

[13] K.N. Son, G.E. Cmarik, J.C. Knox, J.A. Weibel, S.V. Garimella, Measurement and Prediction of the Heat of Adsorption and Equilibrium Concentration of CO2 on Zeolite 13X, Journal of Chemical & Engineering Data 63 (2018) 1663-1674.

[14] J. Choma, K. Stachurska, M. Marszewski, M. Jaroniec, Equilibrium isotherms and isosteric heat for CO2 adsorption on nanoporous carbons from polymers, Adsorption 22 (2016) 581-588.

[15] J.-S. Lee, J.-H. Kim, J.-T. Kim, J.-K. Suh, J.-M. Lee, C.-H. Lee, Adsorption Equilibria of CO2 on Zeolite 13X and Zeolite X/Activated Carbon Composite, Journal of Chemical & Engineering Data 47 (2002) 1237-1242.

[16] R.J. Harper, R. Stifel, R.B. Anderson, Adsorption of gases on 4A synthetic zeolite, The Canadian Journal of Chemical Engineering 47 (1969) 4661-4670.

[17] H. Ahn, J.-H. Moon, S.-H. Hyun, C.-H. Lee, Diffusion Mechanism of Carbon Dioxide in Zeolite 4A and CaX Pellets, Adsorption 10 (2004) 111-128.

[18] R.M. Novais, R.C. Pullar, J.A. Labrincha, Geopolymer foams: An overview of recent advancements, Progress in Materials Science 109 (2020) 100621.

[19] P. Rożek, M. Król, W. Mozgawa, Geopolymer-zeolite composites: A review, Journal of Cleaner Production 230 (2019) 557-579.

[20] A. Natali Murri, F. Miccio, V. Medri, E. Landi, Geopolymer-composites with thermomechanical stability as oxygen carriers for fluidized bed chemical looping combustion with oxygen uncoupling, Chemical Engineering Journal 393 (2020) 124756.
[21] S. Ray, G. Das, Chapter 12 - Adsorption, in: S. Ray, G. Das (Eds.) Process Equipment and Plant Design, Elsevier2020, pp. 351-384.
[22] J. Xiao, Y. Peng, P. Bénard, R. Chahine, Thermal effects on breakthrough curves of pressure swing adsorption for hydrogen purification, International Journal of Hydrogen Energy 41 (2016) 8236-8245.
[23] J.-G. Jee, S.-J. Lee, C.-H. Lee, Comparison of the adsorption dynamics of air on zeolite 5A and carbon molecular sieve beds, Korean Journal of Chemical Engineering 21 (2004) 1183-1192.
[24] D. Leinekugel-le-Cocq, M. Tayakout-Fayolle, Y. Le Gorrec, C. Jallut, A double linear driving force approximation for non-isothermal mass transfer modeling through bi-disperse adsorbents, Chemical Engineering Science 62 (2007) 4040-4053.
[25] E. Papa, V. Medri, S. Amari, J. Manaud, P. Benito, A. Vaccari, E. Landi, Zeolite-geopolymer composite materials: Production and characterization, Journal of Cleaner Production 171 (2018) 76-84.
[26] M. Minelli, M.G. De Angelis, F. Doghieri, M. Rocchetti, A. Montenero, Barrier properties of organic–inorganic hybrid coatings based on polyvinyl alcohol with improved water resistance, Polymer Engineering & Science 50 (2010) 144-153.
[27] B.E. Poling, J.M. Prausnitz, J.P. O'Connell, Properties of Gases and Liquids, Fifth Edition, McGraw-Hill Education, New York, 2001.
[28] R. Sips, On the Structure of a Catalyst Surface, J. Chem. Phys. 16 (1948) 490-495.
[29] K.Y. Foo, B.H. Hameed, Insights into the modeling of adsorption isotherm systems, Chemical Engineering Journal 156 (2010) 2-10.
[30] I. Langmuir, The constitution and fundamental properties of solids and liquids. Part I. Solids, J. Am. Chem. Soc. 38 (1916) 2221-2295.
[31] M. Gholami, M.R. Talaie, Investigation of Simplifying Assumptions in Mathematical Modeling of Natural Gas Dehydration Using Adsorption Process and Introduction of a New Accurate LDF Model, Industrial & Engineering Chemistry Research 49 (2010) 838-846.
[32] L. Hauchhum, P. Mahanta, CO2 Capture onto Zeolite 13X and Zeolite 4A by Pressure Swing Adsorption in a Fixed Bed. , Applied Mechanics and Materials 592-594 (2014) 1456-1460.
[33] J. Davidovits, Geopolymer Chemistry and Applications, 5th ed., Geopolymer Institute, Saint-Quentin (FR), 2008.
[34] E. Landi, V. Medri, E. Papa, J. Dedecek, P. Klein, P. Benito, A. Vaccari, Alkali-bonded ceramics with hierarchical tailored porosity, Applied Clay Science 73 (2013) 56-64.
[35] G. Song, X. Zhu, R. Chen, Q. Liao, Y.-D. Ding, L. Chen, An investigation of CO2 adsorption kinetics on porous magnesium oxide, Chemical Engineering Journal 283 (2016) 175-183.
[36] T.L.P. Dantas, F.M.T. Luna, I.J. Silva Jr, A.E.B. Torres, D.C.S. de Azevedo, A.E. Rodrigues, R.F.P.M. Moreira, Modeling of the fixed - bed adsorption of carbon dioxide and a carbon dioxide - nitrogen mixture on zeolite 13X, Brazilian Journal of Chemical Engineering 28 (2011) 533-544.
[37] C.S. Ellis, J.N. Holsen, Diffusion Coefficients for HE-N2 and N2-CO2 at Elevated Temperatures, Industrial & Engineering Chemistry Fundamentals 8 (1969) 787-791.
[38] R.H. Perry, D.W. Green, J.O. Maloney, Perry's Chemical Engineers' Handbook, Seventh Edition, McGraw Hill, New York, 2007.
[39] S.V. Patankar, Numerical heat transfer and fluid flow, Hemisphere, New York, 1984.